Braz J Phys (2012) 42:292–305
DOI 10.1007/s13538-012-0079-9

SOCIEDADE BRASILEIRA DE FÍSICA

CONDENSED MATTER

Bose–Einstein Condensation of Magnons in $NiCl_2$-4SC$(NH_2)_2$

Armando Paduan-Filho

Received: 26 April 2012 / Published online: 15 May 2012

Abstract A Bose–Einstein condensation (BEC) has been observed in magnetic insulators in the last decade. The condensed bosons are magnons associated with an ordered magnetic phase induced by a magnetic field. We review the experiments in the spin-gap compound $NiCl_2$-4SC$(NH_2)_2$, in which the formation of BEC occurs by applying a magnetic field at low temperatures. This is a contribution to the celebration of the 50th anniversary of the Solid State and Low Temperature Laboratory of the University of São Paulo, where this compound was first magnetically characterized.

Keywords Quantized spin models · Magnetic phase boundaries · Macroscopic quantum phenomena in magnetic systems · Magnetic materials · Bose–Einstein condensation · Magnons

1 Introduction

Macroscopic systems governed by quantum mechanics of interacting particles attract a great deal of interest. Cold atoms and quantum magnets, whose total spin is an integer, have interesting similarities that show the common physics of these two seemingly different realizations [1–11]. All atoms with an even number of neutrons satisfy Bose statistics, which accounts for about 75% of the atoms in the periodic table. Based on the Bose–Einstein statistics a gas of non-interacting massive bosons condenses below a certain temperature T_{BEC}, in which the Bose–Einstein condensation (BEC) occurs. This is a macroscopic quantum phenomenon characterized by spontaneous quantum coherence persisting over macroscopic length and time scales. In dilute atomic gases this phenomenon was realized experimentally for cold atoms. Several quantum spin systems in solids, which show a magnetic-field induced transition, are expected to also show condensation above or below a certain critical field [2, 7, 12]. Studies have shown that the magnetic system can be mapped nonlocally onto a set of weakly interacting bosons on a lattice.

The sorting phase can be described as a BEC of bosonic quasi-particles, in which the magnetic field acts to preserve the number of bosons. Therefore, the tuning parameter to induce condensation in spin-ordered systems is not the temperature, but the magnetic field. For particles as well as magnons, a macroscopic number of bosons condense into a single quantum state—the state of lowest energy. The quantum coherence of Bose–Einstein condensation dates back to the prediction of Einstein, based on Bose's work, in 1924.

In the diluted BEC the macroscopic wave function is directly connected with the microscopic energy levels, providing a complete description of these phenomena in terms of the Gross-Pitaevskii equation. The concept of a coherent macroscopic matter wave in interacting many-body systems is independent of a detailed microscopic understanding of particles. The intricacies of the many-body problem with interactions that lead to nonseparable Hamiltonians are solved by this equation, which introduces effective potentials that are simpler

A. Paduan-Filho (✉)
Instituto de Física, Universidade de São Paulo,
São Paulo, 05314-970 SP, Brazil
e-mail: apaduan@if.usp.br

than the original interactions, which in turn renders the physical problem more tractable.

Experimental evidence of the BEC in confined weakly interacting gases was produced by E. A. Cornell, W. Ketterle, and C. E. Wieman in 1995, leading to a Nobel Prize in 2001. That BEC would occur in quantum magnets was first predicted in 1991, and several reports describing real systems were published after 2000 [7, 13, 14]. The possibility of experimental investigation of the BEC in quantum magnets has led to a deeper understanding of the ground states in strongly correlated systems. Recent studies concerning the BEC of bosons in magnetic systems ranged from a $3D$ weakly coupled $S = 1/2$ dimer compound, $TlCuCl_3$ [7] (the first system in which an identification was attempted with BEC), a quasi-$2D$ spin system, $BaCuSi_2O_6$ [13], to a quasi-$1D$ $S = 1$ chain with single-ion anisotropy, $NiCl_2$-$4SC(NH_2)_2$ (DTN) [14]. In addition to these three compounds, other gapped spin systems share the same physical picture of the BEC, most of which comprise Cu dimers.

The focus of this article is to review systematic concepts and experimental realizations of a transition to a BEC phase in DTN, where bosons are quanta of magnetic excitations in a magnetically ordered ensemble of magnetic moments. Although there is no consensus on a specific name for the magnetic excitations, we will use the word magnon for the excitations in insulating systems generated by the application of a magnetic field. This denomination follows the nomenclature used by the first papers on BEC in magnetic insulators, since elementary excitations in antiferromagnetic systems are called magnons [2, 7].

We hope that the experimental evidence for BEC in DTN will stimulate new research in this fascinating quantum phenomenon.

The outline of this paper is as follows. Section 2 reviews the concepts of the ideal BEC at finite temperature and the nature of BEC when magnons are induced by the application of a magnetic field. Section 3 presents the magnetic properties of DTN, introducing the Hartree–Fock–Popov analysis of the hard-core boson Hamiltonian. Section 4 presents experimental works that lead to the interpretation of the induced phase diagram as a BEC. Section 5 summarizes the results obtained for DTN in the framework of the BEC of magnons.

2 Bose–Einstein Condensation

According to the Heisenberg uncertainly principle the position of a particle is smeared out over a distance given by the thermal *de Broglie* wavelength $\lambda = h/(2\pi m k_B T)^{1/2}$, where k_B is the Boltzmann constant, m is the particle mass, and T is the system temperature [5, 11]. At room temperature λ is typically one hundred thousand times smaller than the average spacing between the particles, a. This means that the matter waves of the individual particles are uncorrelated, and the system can therefore be described by classical Boltzmann statistics. As the system is cooled, eventually the distance between two particles becomes the same as the *de Broglie* wavelength, $a \approx \lambda$ [1, 11]. The packet-functions of adjacent particles overlap, causing the atoms to lose their identity, and the behavior of the system becomes strongly correlated. The system is now governed by quantum statistics. The density distribution of the condensate is represented by a single macroscopic wave function with a well-defined amplitude and phase, which are the order parameters of the system, and a Bose Einstein condensate is formed. Figure 1 shows illustrates this.

The Bose–Einstein condensation is associated with bosonic particles at low temperatures that condensate into a quantum state at a temperature T_{BEC}. At low temperatures, the density of bosons with mass m may

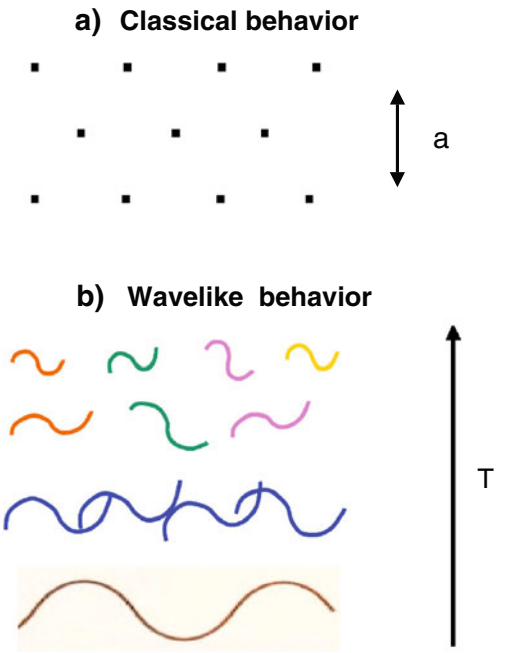

Fig. 1 (*Color online*) **a** Classical representation of a solid. a is the average distance between the particles. **b** In the wavelike representation the position of the particles is given by the thermal *de Broglie* wavelength λ. For decreasing temperatures the wave-packet becomes correlated for $\lambda \approx a$. For particles in the same quantum state, such as bosons at very low temperatures, the system is represented by a single macroscopic wave-function

be expressed by the power-law dependence equation within the BEC picture as

$$\rho = \zeta(3/2)\left(\frac{mk_B}{2\pi\hbar^2}\right)^{3/2} T_{BEC}^{3/2}, \quad (1)$$

where ζ is the Riemann zeta function, and $\zeta(3/2) = 2.612$ [1, 7, 9].

For diluted bosons with small interaction, meaning that the two-particle scattering length x is much shorter than the interatomic distance, the observed T_{BEC} agrees well with the theoretical expectation for free particles. For less diluted systems, the interaction between bosons gives rise to a small shift of T_{BEC} [4, 5]:

$$\Delta(T_{BEC})/T_{BEC} = c\rho^{1/3}x. \quad (2)$$

Various authors have attempted to determine the value of c, which was found to be in the range 1–2, although all authors agree on the functional form.

2.1 Candidates for BEC

There are several candidates for BEC. A first attempt to experimentally observe BEC was made with superfluidity. When ^{4}He is cooled to a critical temperature of 2.17 K, the liquid density drops, and fractions of the liquid become superfluid. The strong interaction of ^{4}He in liquid form prevents perfect condensation. The formation of Cooper pairs of electrons, which act like bosons, is also evidence of the condensation effect, which produces superconductivity [1, 15]. However, in these systems, a macroscopic wave function provides only a phenomenological description of the superfluid state.

By contrast, the macroscopic wave function of pure condensates is directly connected with the microscopic degrees of freedom, providing a complete and quantitative description of both static and dynamic phenomena. This description should cover systems showing a true BEC phase. Some systems were cited, such as excitons-polaritons, which are light-mass quasi-particles usually produced by optical excitations in semiconductors, and photons confined in a cavity [1, 11, 15–17]. However, excitons have a very short lifetime and the photons are absorbed by the walls. Because the BEC requires a thermalization time to condense in which the number of particles is conserved, their characteristics almost prevent these systems from becoming BECs. All these systems are believed to be defective condensates.

Recently it has been reported that a gas of magnons at room temperature can be continuously overpopulating the lowest energy level, which shows characteristics of BEC, when it is driven by microwave pumping [18, 19].

On the other hand, diluted magnons in equilibrium can be pure condensates at low temperatures, just like cold gas.

2.2 BEC of Magnons

Magnetic insulators with magnetic ions are characterized by a gap separating the singlet ground state from the lowest-energy excited state. If the gap is closed by the Zeeman effect, the resulting quasiparticles can undergo the Bose–Einstein condensation transition.

The BEC phase in quantum magnets is an XY antiferromagnetic state in which the spins spontaneously choose a particular orientation in the XY plane. The number of bosons is proportional to the net magnetization, i.e., the S^z component of the spins. On the other hand, the number of condensed bosons is proportional to the antiferromagnetically ordered S^x component of the spins. Thus the XY antiferromagnetic order parameter maps directly onto the order parameter for Bose–Einstein condensation. It has a magnitude (size of the spins in the spin language, or number of bosons in the boson language) as well as a phase (direction of the spins). In the particle language, the boson number can be tuned by the magnetic field. For this to occur, the system must be an XY magnet, i.e., must have uniaxial symmetry in the plane perpendicular to the applied magnetic field. Therefore only certain quantum magnets can be treated as BECs. We note that in real systems there will always be terms that break the uniaxial symmetry, such as dipole-dipole interactions and spin-orbit interactions. Consequently the theory is valid only when these terms are significantly smaller than the temperature. At very low temperatures any real quantum magnet will cross over to the Ising universality class.

Bosons can be achieved by creating and maintaining a large number of quasi-particles in a system. One special case is the creation of magnons at the induced magnetic-ordering phase. Figure 2 shows the phase diagram in the temperature-versus field plane of an induced antiferromagnetic ordering in a field whose magnetic ions are strongly correlated. Magnons can be created and, under special conditions, condensed into the ordered phase [2, 8, 14].

A procedure for studying the properties of the phase diagram is to understand the transitions that appear when the boundaries separating the phases are crossed ([7, 20, 21], V.S. Zapf, unpublished). When a border is crossed vertically to enter the ordered phase a thermal

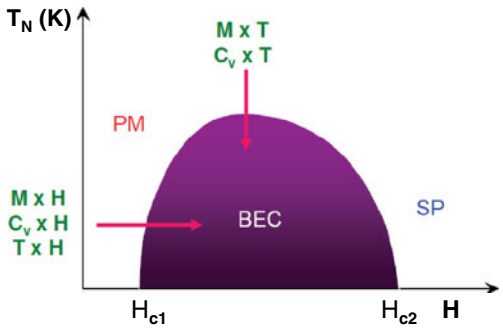

Fig. 2 (*Color online*) The phase diagram from the normal to the BEC state can be studied via thermodynamic properties such as magnetization, temperature and specific heat, which are measured when the phase boundary is crossed by sweeping the field or the temperature, as indicated by the *arrows*

phase transition results, driven by thermal fluctuations. The magnetic and thermal energies compete. At temperatures near zero, by contrast, there are no thermal fluctuations and a quantum transition results, driven by quantum fluctuations. The magnetic energy and the zero-point energies compete. This second-order quantum transition to the BEC phase is free of interactions. However, including even week interactions into the description of the condensation has proven to be a great challenge, which was overcome by introducting effective interactions [7, 10, 20, 21]. These interactions, well-approximated by a contact pseudo-potential, are central to arriving at the Gross-Pitaevskii equation. Understanding the behavior of the phase transition near zero temperature is understanding the quantum behavior of the system. The transition to the BEC state is characterized by specific characteristics of the thermodynamic properties.

We studied BEC in magnons because condensation occurs at temperatures that are much more accessible than the condensation of particles.

Since according to (1) T_{BEC} is proportional to $\rho^{2/3}/m$, we would like to maximize ρ to observe the BEC at easily accessible temperatures. However, that equation assumes that the bosons are free particles and is therefore only valid in the limit of low density. We can overcome this problem by considering that T_{BEC} is also dependent on the boson mass m. By minimizing m, we can observe the BEC at relatively high temperatures without sacrificing the condition of low boson density. In quantum magnets, the boson mass is sufficiently small, so that the BEC can be realized at temperatures of a few Kelvin, in contrast to cold atoms, in which temperatures in the nano-Kelvin range are needed to observe the BEC in magnetic optical traps [19, 21].

3 Magnetic Properties of DTN-BEC

In addition to the properties of $NiCl_2$-$4SC(NH_2)_2$, one needs well-prepared samples for studies under laboratory conditions. Single crystals of dichloro-*tetrakis*thiourea-nickel (DTN) were grown by dissolving a large excess of nickel chloride in a saturated solution of thiourea [22]. The crystals grow after about two weeks in a solution maintained at a temperature of 35 degrees centigrade. Yellow-brown single crystals are tetragonal prisms along the *c*-axis (Fig. 3a). The space group of DTN is $I4$, with two molecules in the unit cell, whose dimensions are $a = b = 9.558$ Å and $c = 8.981$ Å. The $S = 1$ Ni atoms form two interpenetrating tetragonal lattices. The thioureas are bounded to the nickel by means of the sulfur atoms in a square array. The spin must be in an environment of approximate uniaxial symmetry (Fig. 3b). The metal is in a non-centrosymmetric environment of fourfold symmetry. All molecules are oriented in the same way and held together by Cl-N hydrogen bonds. The Cl-Ni-Cl axes all lie parallel to the crystal *c*-axis. The samples were always chemically analyzed for their main constituents. Polarized light allowed us to verify the excellent quality of the samples and to check the orientation of the crystallographic axes for the measurements, as determined by *X*-ray. The sample masses in our experiments ranged from a few milligrams to 2 g.

Initially, to provide magnetic characterization, the magnetic susceptibitilies of a single crystal were measured in the directions parallel and perpendicular to the *c*-axis, and temperatures ranging from 0.4 to 300K.

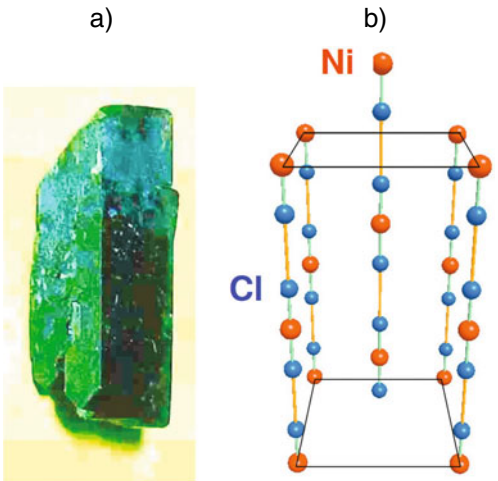

Fig. 3 (*Color online*) **a** Sample of DTN grown in water solution. **b** Schematic crystal structure of the compound. The positions of the Ni and Cl atoms are shown

From these data the parameters applicable to the following $S = 1$ spin-Hamiltonian with single-ion anisotropy were determined:

$$\mathcal{H} = \sum_{\mathbf{j},\nu} J_\nu \mathbf{S}_\mathbf{j} \cdot \mathbf{S}_{\mathbf{j}+e_\nu} + \sum_\mathbf{j} \left[D(S^z_\mathbf{j})^2 - g\mu_B H S^z_\mathbf{j} \right]. \quad (3)$$

The obtained parameters are $g = 2.30$ and $D \approx 9$K. Molecular field correction gives the exchange interaction parameter $J \approx -2.2$K (antiferromagnetic). The high D value and the anisotropy in the exchange suggest a quasi 1D behavior. These data were used to anticipate an induced ordered phase at low temperature in an applied magnetic field below $\approx$ 11 T.

3.1 Magnetic Induced Phase Diagram—BEC

The field-induced phase by level crossing is permitted in compounds that follow stringent requirements: in addition to having a multiplet above the non-magnetic singlet, the metal ion must reside in a site of uniaxial symmetry, so that the magnetic field can be applied simultaneously parallel to the anisotropic z axis for all magnetic ions. The parameters for DTN and its crystal symmetry then yield magnetic properties that can be studied within this picture.

In DTN the high single-ion anisotropy (energy gap) is responsible for the splitting of the $S = 1$ spin triplet of the Ni^{2+} in a $S^z = 0$ ground state and an $S^z = \pm 1$ excited doublet considerably higher in energy. The excited doublet can hop to a neighboring doublet via the transverse component of the magnetic exchange interaction J, resulting in delocalized states analogous to the delocalized electronic states in crystals. At zero field the small exchange interaction between the spins is not enough to induce long-range ordering, even at zero temperature. The application of a magnetic field H leads to a splitting of the doublet, which brings down the component parallel to the field linearly with H until the gap between the excited and ground states closes at $H = H_c$. At this point magnetic excitations, i.e., bosons, are created (Fig. 4a).

The more realistic view of the energy levels that takes the interaction into account is shown in Fig. 4b. The exchange interaction produces a dispersion of the energy levels, and there is now a field range, from H_{c1} to H_{c2}, where the $S^z = +1$ level becomes degenerate with the ground state and bosons are created. This gapless phase extends throughout this field range. The coupling to the magnetic field, which is proportional to the magnetization, controls the boson density. The BEC that appears in this intermediate field range corresponds to the coherent superposition of the $S^z = +1$ doublet and the $S = 0$ singlet at each site ([14, 22, 23], V.S. Zapf, unpublished).

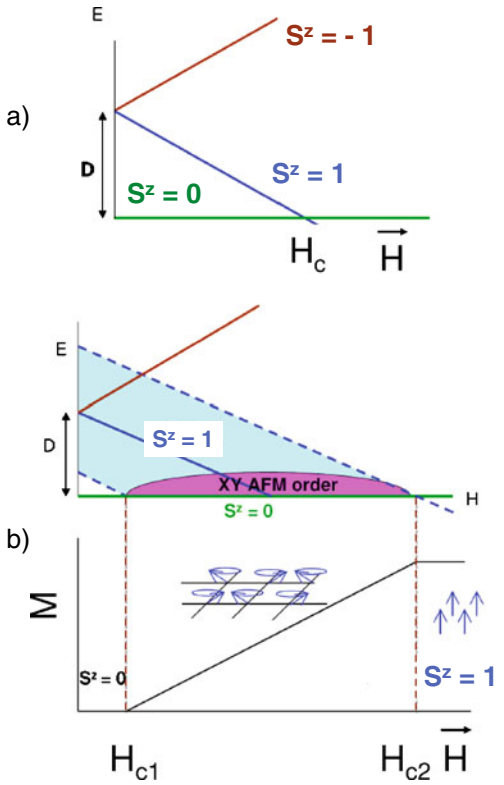

Fig. 4 (*Color online*) Schematic diagram ($T = 0$) of the levels of energy. **a** The lowest energy levels of Ni^{++} in an axial crystalline field as a function of the external magnetic field. **b** The broad band indicates dispersion of the lowest excited level due to exchange coupling. Condensation occurs in the range between the fields H_{c1} and H_{c2}, in which the magnetization M increases almost linearly up to the saturation

The transition to the magnetic phase can be adequately described as a condensation of bosons. Three are the basic conditions for BEC induced by a magnetic field: (1) the excited state becoming degenerate with the ground state, (2) strong correlation inducing 3D long-range ordering, and (3) a uniaxial symmetry leading to number conservation of bosons.

3.2 Hard-Core Boson Model

The first attempt to interpret a field-induced phase ordering in a BEC was made by Nikuni [7]. In his work the induced phase diagram of $TlCuCl_3$ was studied by applying the Hartree–Fock–Popov (HFP) mean field analysis to the hard-core boson Hamiltonian. For a diluted gas of particles the interatomic interaction is sufficiently weak, therefore the mean field Gross–Pitaevskii theory is a logical tool to study this system. In this model the particle scattering is dominated by the

two-body contact interactions, which are described by the *s*-wave scattering length. The physical implication of this condition is that it is highly improbable for more particles to interact with each other simultaneously. In hard-sphere gas, the scattering length is equal to the diameter of the atoms. In the low-density limit only the two particles interactions are important. The low-energy Hamiltonian (3) can be transformed into boson language via identifying $S^+ = a^\dagger$, where $a^\dagger$ is the boson creation operator, in

$$\mathcal{H} = \sum_k (\epsilon - \mu))a_k^+ a_k + \frac{v_0}{V} \sum a_{k+q}^+ a_{k-q}^+ a_k a_k \tag{4}$$

where $\epsilon = \hbar k^2/2m$ is the kinetic energy, v_0 is the short-range repulsion between two magnons that occupy the same site and V is the unit-cell volume of the sample.

In this hard-core model applied to the Ni^{2+} ions the density of the magnetization along the field direction, $S^z = +1$, is mapped onto the boson density. Here the $S^z = -1$ component is neglected, because we are interested in low-field and low-temperatures regions, where this level does not contribute. An analysis taking this level into account is discussed in Section 4.17 ([14], V.S. Zapf, unpublished).

The physics of the magnons depends on the relative strengths of the repulsive interaction v_0 and kinetic energy. When the interaction is attractive, $v_0 < 0$, the system collapses. If the repulsion interaction dominates, the system evolves into a state where the bosons form a large lattice that gives rise to a magnetization plateau in the M *vs*. H curve. If the kinetic term dominates, the system, which corresponds to a Mott insulator in the low-field region, undergoes a condensation at the first critical field H_{c1}. Above this field the density of bosons increases proportionally to the longitudinal component of the magnetization M up to the saturation value, M_{sat}, at the second critical field H_{c2}. The result is an antiferromagnetic state characterized by the presence of a staggered transverse moment, M_{sta}, perpendicular to the applied magnetic field, forming a BEC state. The absolute value and relative angle of M_{sta} are related to the amplitude and the phase of the condensate wave function, respectively. In this phase the condensate shows a macroscopic order parameter that spontaneously breaks global phase symmetry by the emerging antiferromagnetic longe-range order. In these conditions, there must exist a gapless mode called Nambu–Goldstone in the new phase, which is necessary to keep the original invariance of the Hamiltonian. At H_{c2} all sites are occupied by bosons and the system enters a second Mott insulating phase [24–27].

3.3 Boson Number Conservation

At the induced phase the Ni magnetic spins do not have any preferred orientation in the plane perpendicular to the magnetic field, and the antiferromagnetic order is XY-like. The tetragonal crystal structure provides a uniaxial crystal-field symmetry about the direction of the applied field. It is this symmetry that enforces number conservation among the bosons. This forces the bosons to remain in the system and macroscopically occupy the ground state at low temperatures. Boson-number conservation is a key condition that separates bosonic systems that condense from those that do not. Formally, the phenomenon of BEC requires the conservation of particle number. The boson number must be set by some external constraint or else bosons will be excitations of the system and vanish as the temperature is lowered to zero, as is the case, e.g., for phonons. In the Hamiltonian (4) every creation operator $a^\dagger$ is multiplied by a destruction operator a. If the Hamiltonian is rotated by an angle ϕ in the plane perpendicular to the field, then $a^\dagger \to a^\dagger e^{i\phi}$ and $a \to ae^{-i\phi}$, such that $(a^\dagger e^{i\phi})(ae^{-i\phi}) = a^\dagger a$. Because this Hamiltonian is independent of ϕ the number of bosons is conserved. Thus, the uniaxial symmetry of the Hamiltonian creates a number conservation law for the bosons [28]. In real situations, the square lattice of the crystal can introduce a small anisotropy in the *ab* plane along with dipole-dipole interactions or Dzyaloshinskii–Moriya (DM) interactions. These effects generally occur at lower energy scales and can therefore be neglected at the temperatures at which DTN was studied. [21] However, experimental studies should be conducted to discard effects of this possible anisotropy in the formation of BECs.

3.4 Low-Temperature Limit and Critical Behavior

The self-consistent HFP approximation leads to the following effective Hamiltonian for the magnon system:

$$\mathcal{H} = \sum_k (\epsilon - \mu + v_0 n)\, a_k^+ a_k, \tag{5}$$

where n is the density of bosons per magnetic ion, given by $n = M/M_{sat}$.

The chemical potential

$$\mu = g\mu_B(H - H_c) \tag{6}$$

determining the number of bosons in the ground state characterizes an additional direct contribution to the magnon energy from the external field H.

Bosons condense when the renormalized effective chemical potential is zero [3, 7, 29] (Fig. 5):

$$\mu_{eff} = \mu - 2v_0 n = 0; \tag{7}$$

the factor of two comes from exchange.

At this "point of condensation", where the gap is closed, the applied magnetic field is responsible for driving the system to the BEC phase in which bosons are created at (H_{c1}, T_{c1}). At H_{c1} the magnetization acquires the value $M_c(T)$ and $n_c(T) = M_c(T)/M_{sat}$ gives the number of bosons created at the transition. Using (6) and (7), the low-field boundary of the phase diagram H *vs.* T can be written as [3, 20, 21, 24, 25]

$$H_c(T) - H_c(0) = \left[2v_0/g\mu_B\right] n_c(T). \tag{8}$$

On the other hand, the density of created bosons is given by Bose–Einstein statistics

$$\rho(T) = (1/V) \sum_{\mathbf{k}} \left[1/\left[\exp(\epsilon_k/T) - 1\right]\right] \tag{9}$$

That is, at the low-temperature limit [1, 7, 9, 31] and letting the chemical potential be μ_{eff}:

$$\rho(T) \approx \zeta(3/2) \left(\frac{mk_B T}{2\pi\hbar^2}\right)^{3/2}, \tag{10}$$

since the density of bosons per magnetic ion is $n_c(T) = \rho(T)V$, where V is the unit cell volume, (8) becomes

$$H_c(T) - H_c(0) \approx \left[2v_0/g\mu_B\right] \zeta(3/2) \left(\frac{mk_B T}{2\pi\hbar^2}\right)^{3/2} V. \tag{11}$$

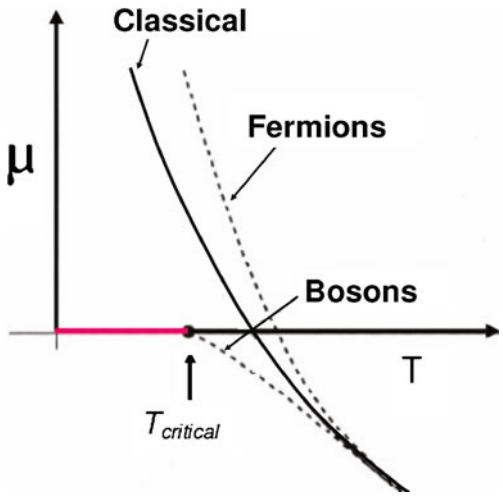

Fig. 5 (*Color online*) Effective chemical potential as a function of temperature for fermions, bosons and classical particles. For decreasing temperatures, μ for bosons reaches the zero limit at the temperature T_{critical}. As T becomes lower than T_{critical}, μ is pinned at zero [30]

3.5 Signature of the BEC

Based on this analysis, the phase boundary can be interpreted as a BEC of magnons. At low temperatures only the lowest excited energy level is considered, so that the interaction can be replaced by the constant v_0. In this case, introducing a hard-core constraint assuming an infinite on-site repulsion, only one boson occupies each site. Certain properties of the induced magnetic phase in $TlCuCl_3$ can be explained by the concept of a BEC. Plotted as a function of the field, the magnetization shows the cusplike dip at the transition predicted by HFP theory [7, 20, 25]. However, disagreements are found with other experiments, wich were later attributed to the lack of uniaxial symmetry.

One of the few compounds entering the BEC phase under magnetic fields sufficiently low to be reached using standard superconducting magnets is DTN. Most other candidates require pulsed fields and yield much less accurate experimental results. To condensate at $T \neq 0$, magnons should be able to propagate in three dimensions. For BEC to occur in quasi-1D system, such as DTN, there must be weak interaction between the 1D chains, which permits full mobility of magnons in 3D.

One of the experimental features of the BEC of magnons can be found by analyzing the experimental data at the boundary $H_{c1}(T)$, where part of the excitations condense.

The signature of the BEC universality class at low temperature is given by the power-law [3, 7, 12, 20, 21, 24, 25]

$$H_{c1}(T) - H_{c1}(0) \approx \ AT^{\phi}, \tag{12}$$

where A is fully determined by the coefficient of (11) as a function of v_0 and the mass of magnons.

DTN behaves in 3D below 1.2K as a BEC, which is where the long-range order sets in, although the universal behavior with $\phi = 3/2$ is observed only below $T <$ 0.2K. This is because the $\phi = 3/2$ power-law behavior is a low-temperature approximation to the full boson distribution function.

4 Experimental Determination of the BEC Phase

A wealth of useful information about the nature of the transition to the ordered phase can be obtained from several thermodynamics properties in the temperature *vs.* field plane (Fig. 2). The first thermodynamic property used to study the transitions is the magnetization, one of the most fundamental quantities observed in experiments, followed by specific heat and

magnetocaloric effect. More properties such as magnetostriction, thermal transport, EPR, inelastic neutron scattering, and other techniques are used to identify the induced magnetic phase as BEC.

4.1 Magnetization

The boundary of the induced phase diagram of DTN can be experimentally determined by curves of magnetization *vs*. temperature at fixed H, with a cusp-like minimum at T_c, or by H_c at the inflexion in scans of magnetization at fixed temperature T. These critical points originate from the competition of two behaviors of the magnetization, which correspond to the number of magnons: above T_c, magnetization is determined by the number of thermally excited magnons, which decreases with decreasing T; below T_c the number of condensed magnons increases with decreasing temperature, overcoming the decrease of thermally excited magnons. As a result of this competition on the origin of the magnons, M has a minimum at T_c, with the value M_c (Fig. 6a). For the same reason, when the phase boundary is crossed by sweeping H at a fixed temperature, the condensation occurs at the inflexion field H_c (Fig. 6b). It has been proved that at $H_c(T_c)$ a discontinuity of the magnetization is provided by the sudden vanishing of the chemical potential μ [7, 20, 24, 25, 27].

The magnetization was measured using a vibrating sample magnetometer, VSM, in temperatures above 0.4K at the High Magnetic Field Laboratory facility of the University of São Paulo. The sample was immersed in a ^{3}He bath, and the temperature was measured by vapor pressure and carbon-glass or Cernox thermometer. The magnetic field was supplied by a Nb_3Sn superconductor. Measurement at $T = 0.019$K was made using the gradient field method in the dilution refrigerator. The transitions were determined in the magnetization versus field curves by locating anomalies in the second derivative of the magnetization [32].

4.2 Specific Heat

All measurements were made on crystals with the external field H provided by the 17–20 T superconducting magnet in a dilution refrigerator system at the National High Magnetic Field Laboratory in Los Alamos. The magnetic field was always applied along the tetragonal c-axis of the sample. Specific heat was measured with two methods, as shown in Fig. 7.

Measurements at quasi-constant temperature were made using a developed ac technique, Fig. 7a. A small sample, ≈1 mg, was mounted onto a home-made calorimeter consisting of a Si platform furbished with an amorphous-metal thin film heater and a bare Cernox thermometer. The calorimeter was attached to the temperature regulation block and was held in a cryogenic vacuum system inside a refrigerator. The sample heater is driven by one lock-in amplifier running at frequency f, and the temperature is detected with a second lock-in locked to the frequency of $2f$. In both cases a peak is observed at the transitions. The observed anomalies in C_p map the known phase boundaries in DTN quite well. In the C_p versus H curves a double peak is apparent, with the peak near H_{c2} far larger than the peak near H_{c1}. A comprehensive theory of the specific heat has been developed. Quantum fluctuations present near H_{c1}, but not near H_{c2}, reduce the kinetic energy of the magnons, causing a strong mass renormalization near the two transitions, $m(H_2)/m(H_1) \approx 3$. This effect, closely described by analytical and quantum Monte Carlo calculations, explains similar asymmetries observed in other properties of DTN, such as magnetization, electron spin resonance, magnetostriction, and thermal conductivity [33].

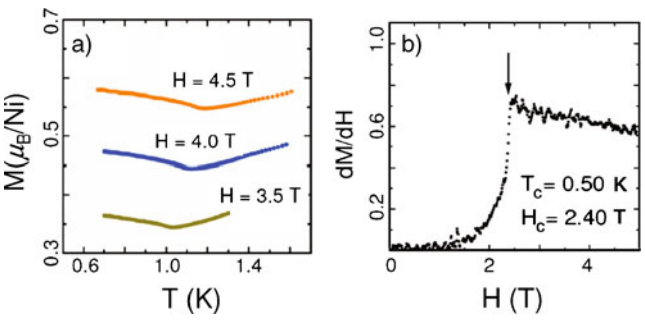

Fig. 6 (*Color online*) **a** Curves of magnetization taken at several fields. The minimum indicates the transition temperature T_c. **b** Representative curve of dM/dH. The sharp bending indicates the transition field H_c

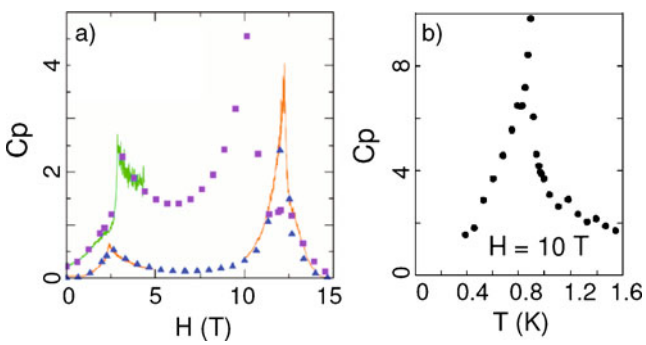

Fig. 7 (*Color online*) **a** Specific heat as a function of the magnetic field for fixed temperatures of 0.40K (*triangles*) and 0.75K (*squares*). **b** Specific heat in an applied field of 10 T

At constant field the method used was the quasiadiabatic heat pulse relaxation technique (Fig. 7b). The sample was mounted onto a sapphire plate and its temperature wa s monitored by a RuO_2 field-calibrated thermometer [14].

4.3 Magnetocaloric Effect

This effect was measured by sweeping the field up and down while monitoring the sample temperature with the bath temperature held fixed. The device was the same that was described in measurements of C_p by the relaxation technique [14]. In the magnetocaloric effect, whose data we show in Fig. 8a, heating is observed as the magnetic field is swept through the boundary of the phase diagram, surrounded by regions of cooling before and after the transition. The peak in the first derivative of $T(H)$, Fig. 8b, corresponding to the maximum heating of the sample, was identified as the phase transition.

4.4 Phase Diagram

The induced ordered phase in the field range $H_{c1} < H < H_{c2}$ extends to a finite temperature $T_c(H)$ in which the maximum temperature for DTN is $T_{\max} = 1.2$K. The thermal and quantum phase transitions are qualitatively different. In the field-induced quantum critical point, the magnetic order is suppressed by both the phase and the amplitude fluctuations. Figure 9 shows the constructed phase diagram.

The measured thermodynamic properties of DTN $C_p(H, T)$, $M(H, T)$, $\Delta T(H)$, used to characterize the transitions, were analyzed in regions near the phase boundaries, the critical regions, to confirm that this is a phase transition to a BEC. Very few quantum magnet

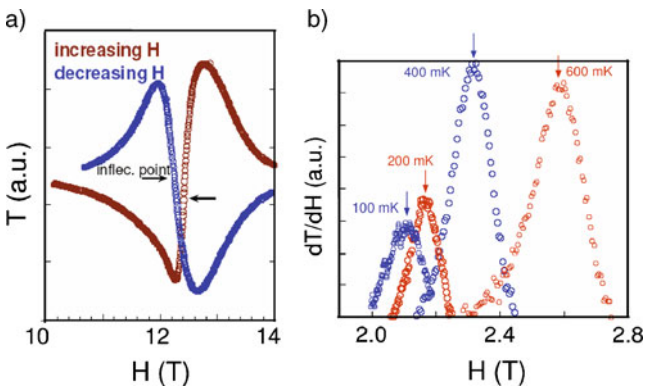

Fig. 8 (*Color online*) **a** Magnetocaloric effect determined by monitoring T while sweeping H up and down. **b** Derivative dT/dH for several temperatures, where the transition is identified as the peak

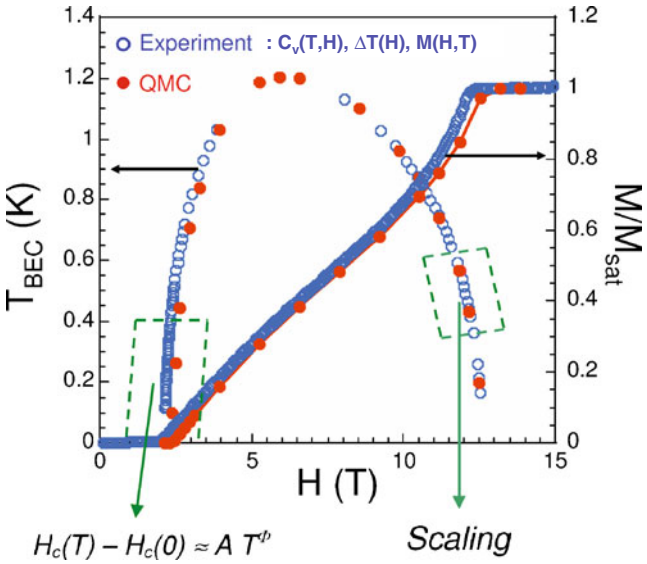

Fig. 9 (*Color online*) Magnetic phase diagram determined from specific heat, magnetocaloric effect, and quantum Monte Carlo simulations (QMC). The magnetization *vs.* field measured at 19 mK and calculated from QMC simulations are overlaid on the phase diagram [14]

candidates to BEC have been studied at temperatures in which the power-law dependence can be confirmed. If the temperature range in which the power-law fit is performed is far from zero temperature, it is difficult to accurately identify the power-law behavior with correct parameters. For example, the first determination of the exponent in DTN yielded $\phi \approx 2$, very different from the expected value [23]. This problem can be circumvented by the windowing method, in which the intercept and the exponent are determined independently by performing fits over different temperature ranges and extrapolating the values to zero temperature. The results show that the field-temperature phase boundary approaches a power law near the quantum critical point, with an exponent value $\phi \approx 1.5$, as expected for $3D$ BEC [14].

Using the theoretical prediction obtained for the scaling form of the field- and temperature-dependent magnetization close to $H_{c2}(T)$, an analysis of the magnetization shows a good agreement between the theoretical and experimental results. This clearly shows that the transition at $H_{c2}(T)$ is a BEC of magnons [34].

4.5 Neutron Scattering

A microscopic understanding of the ground state was reached through inelastic neutron measurements. Low-energy magnetic excitations were performed using the cold neutron triple-axis spectrometer at the Paul

Scherrer Institute, Switzerland. Using an Oxford instruments dilution insert in a VARIOX cryostat, a sample of three co-aligned deuterated single crystals of DTN with a combined mass of 3g were cooled to $T =$ 80 mK. The analysis of the resulting dispersion of the magnetic excitation was adjusted to the Hamiltonian with interaction. The observed scattering was analyzed using a single-mode cross section with dispersion obtained from a generalized spin-wave approach for the disordered phase. The obtained parameters agree with a model of spins of Ni ions strongly coupled along the tetragonal axis, but only weakly perpendicular to it, making DTN a weakly coupled chain system with an anisotropy higher than the exchange interactions [14].

4.6 Electron Spin Resonance

We availed ourselves of the high-field approach exact theoretical expressions for the spin-polarized phase. Investigating magnon excitations in fields up to 25 T allowed us to obtain a reliable set of spin-Hamiltonian parameters. Part of this work was performed at the National High Magnetic Field Laboratory, Tallahassee. The parameters agree very well with those obtained from fitting the experimentally induced phase boundary and low-temperature magnetization of DTN with results of quantum Monte Carlo simulation. The parameters were used to calculate the frequency-field dependence of two magnon bound-state excitations predicted by theory, and observed in DTN for the first time [35–37].

4.7 Four Sublattice Model

We present the low-energy excitation spectrum in the magnetically ordered phase obtained from spin resonance measurements down to 0.45 K. The EPR measurements were made at the Kapitza Institute using a transmission-type spectrometer equipped with a cylindrical multimode resonator and a ^{3}He cryostat. The observed modes can be interpreted within a four-sublattice antiferromagnetic model with a finite interaction between two tetragonal subsystems, $V_{\text{intra-sub}}$ [35].

4.8 Crossover from the 1D Fermionic to the 3D Bosonic Character in DTN

Magnetoacoustic studies in the vicinity of the quantum critical points in DTN show that the behavior of the observed properties outside the ordered phase boundary can be well described by an effective 1D fermionic model of low-lying spin excitons. This, together with previous results showing the bosonic behavior inside the boundary, suggests a crossover from the bosonic to the fermionic character of the magnetic excitations close to the quantum critical points. One fascinating aspect of this crossover is continuous tuning from the bosonic to the fermionic statistics. This research was conducted in Dresden [38].

4.9 Critical Behavior at the Low Field Transition

Interpretating the low-field phase boundary as a transition to the BEC phase allows one to obtain information about the boson interaction in DTN.

The critical field H_c, plotted as a function of n_c in Fig. 10a, follows the linear relation in (8). The interaction strength constant v_0 in that equation can be obtained from the derivative of the fitted curve $dH_c/dn_c = 9.52 = 2v_0/g\mu_B = B$ as $v_0 = 0.61$ meV. The zero temperature transition field is obtained as $H_c(0) =$ 2.15 T, in close agreement with Ref. [14]. This confirms

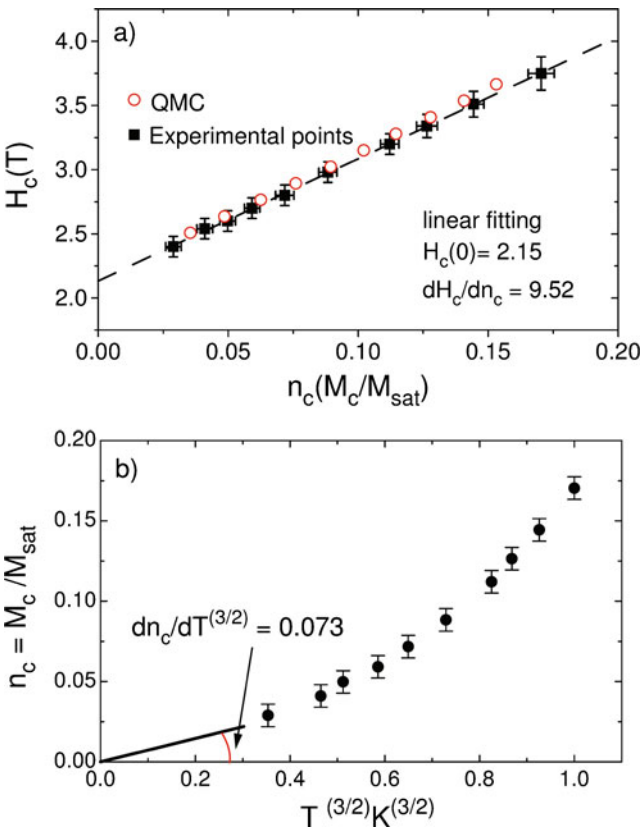

Fig. 10 (*Color online*) **a** Critical transition field as a function of critical magnetization density n_c. The *filled squares* represent the measurements. The *dashed line* denotes the linear fitting of the data. The Quantum Monte Carlo data are shown as *red circles*. **b** n_c as a function of $T^{3/2}$. The *straight line* is the plot of $dn_c/dT^{3/2} = A/B = 0.073$, obtained from (8) and (12) from different experiments. The continuity of this derivative with the experimental points is very high [39]

the behavior is linear over the entire temperature range. Using the value of $A \approx 0.70(T/K^{3/2})$, as obtained from the phase diagram at low temperature, and $B = 9.52$, (8) and (12) simultaneously yield the derivative $dn_c/dT^{3/2} = A/B = 0.073$, which is plotted in Fig. 10b as a straight line. The continuity of this line at low temperature, with the experimental points at high temperature, is a robust indication that the theory is sufficiently coherent to allow us to combine results from different sets of experimental data [21, 39].

4.10 Boson Number Conservation

The derivative dM/dH in Fig. 6b shows a sharp kink at H_c. In a recent report, a Dzyaloshinskii–Moriya (DM) interaction in DTN was proposed to explain the extra lines in ESR experiments. This anisotropic interaction between corner-center coupling spins at sites i, j in the body-centered tetragonal lattice of DTN is given by $\sim \boldsymbol{d} \cdot (\boldsymbol{S}_i \times \boldsymbol{S}_j)$, where $\boldsymbol{d}$ is a specific vector coefficient. For any possible DM interaction, the vector $\boldsymbol{d}$ would have to point along the tetragonal axis. Otherwise a nonuniform field distribution would exist in the sample, which would induce a staggered moment perpendicular to the applied field, which in turn would broaden the magnetization at the transition. This configuration characterizes a broken axial symmetry, as is observed in $TlCuCl_3$. Traces of M *vs*. H are the best for analyzing the configuration of the vector $\boldsymbol{d}$ in DTN. From the sharp peak in d^2M/dH^2 at the transition, we conclude that any possible $U(1)$ symmetry-breaking terms are small at these temperatures, and the number of bosons is conserved, as required for BEC [21].

4.11 Magnetostriction

Magnetostriction taken at dilution refrigerator temperatures, performed in a titanium dilatometer, shows significant magnetoelastic coupling and a magneto-order-induced modification of the lattice parameters in DTN. Length changes were monitored capacitatively with a Be-Cu spring-mounted titanium tip in a plastic rotator. The top-load dilution refrigerator was mounted in a 20 T superconductor magnet system at the National High Magnetic Field Laboratory in Tallahasse. A simple theory relates the magnetostriction to the spin-spin correlation function and describes the data remarkably well. From this, was possible extract the spatial dependence of the magnetic exchange coupling. The measured data agree excellently with those obtained from quantum Monte-Carlo simulations and with the phase diagram determined from C_p and magnetostriction [40].

4.12 Direct Measurement of the BEC Universality Class

Although the windowing method yields the critical exponent at zero temperature by an efficient extrapolation procedure, the physics that can appear below the studied temperatures can be hidden by this method. This was clearly demonstrated for $BaCuSi_2O_6$, in which a reduction in dimensionality of the spin system changed the exponent, as was observed at the lowest temperature. In DTN new measurements were performed at temperatures down to 1 mK, which is two orders of magnitude below the lowest temperature scale for magnetic coupling in this system, $J_{ab} = 0.18$K, and the lowest ever used to investigate BEC in a quantum magnet. Thus, with this new experiment, no extrapolation was needed to determine the power-law exponent. Measurements of the transition were carried out using ac susceptibility. The experiments were performed using a $PrNi_5$ nuclear refrigerator and a 15 T magnet at the National High Magnetic Field Laboratory Facility at the University of Florida. The sample was immersed in liquid ^{3}He in a polycarbonate cell, rather than being glued to a cold finger, and thermal contact to the refrigerator was assured via sintered silver. The temperature was calibrated using a ^{3}He melting-pressure curve thermometer. The device used for operation at ultra-low temperatures is the mutual inductance bridge assembly. The transitions were determined by the derivative of the susceptibility curve. The power-law temperature dependence of the phase transition line, with $\phi = 3/2$, was found to be consistent with the $3D$ BEC universality class, which confirms the conclusion obtained by the windowing method [41].

4.13 Disorder in the Doped System DTN/Br

When disorder is introduced in a magnet with interacting bosons, the condensate disrupts and interferes with phase coherence. The result is the creation of a peculiar state, the Bose-glass phase (BG), with only short-range correlation. In the presence of disorder the transition to BEC is argued to occur only from the BG, and never from the Mott insulator. The transitions to BEC should be governed by physical parameters characteristic for BG $\rightarrow$ BEC for the low-field transition and for BEC $\rightarrow$ BG for the high-field transition. Experimental and theoretical studies were realized in the disorder quantum magnet DTN/Br, $Ni(Cl_{1-x}Br_x)_2$-$4SC(NH_2)_2$. The remarkable agreement between theory and experiment shows a well-controlled realization of a disordered Bose fluid with a new seemingly

universal exponent governing the scaling of the critical temperature from BG to BEC [42, 43].

4.14 Mass of Magnons

From the linear behavior of n_c at low temperatures in Fig. 10b, the effective mass of the bosons in DTN, m_b, can be calculated with the coefficient $dn_c/dT^{3/2}$ from (8) and (11):

$$dn_c/dT^{3/2} = \zeta(3/2)\left(\frac{m_b k_B}{2\pi\hbar^2}\right)^{3/2} V = 0.073. \tag{13}$$

The obtained value is $m_b = 5.4 \times 10^{-25}$ g, which is approximately 1/3 of the proton mass. The value for m_b can be compared with that obtained from neutron dispersion data, $m = 3.7 \times 10^{-25}$ g ([44], A. Paduan-Filho, unpublished).

4.15 Quantum Depletion of Magnons

Although the repulsive interaction between bosons are essential to avoid the collapse of particles, v_0 depletes the number of condensed bosons by the quantity of non-condensed bosons. This was described by Nikuni, who obtained the density of bosons in the BEC phase from the sum of the condensed and the non-condensed densities. To determine the fraction of condensed bosons, we analyzed the n *vs.* H curve at $T = 0.019$K in Fig. 11, which is reasonable approximation to the $T \to 0$ limit. The relation between the total density of particles n and the density of condensed bosons n_{cond}, as an effect of v_0, is given at zero temperature by the equality

$$n(0) = n_{cond}(0) + \frac{1}{3\pi^2}\left(\frac{m v_0 n_{cond}(0)}{\hbar^2}\right)^{3/2} \tag{14}$$

The second term on the right-hand side of this equation represents the number of condensed bosons that are scattered out of the ground state due to interaction v_0. The non-condensed fraction at $T = 0$, called quantum depletion, δn, is caused by quantum fluctuations around the true condensate. Applying (14) to the experimental data we determined the dependence of the condensed bosons with the magnetic field. The open circles in Fig. 11 show the calculated density of condensed bosons. The depletion of condensed bosons just above the critical field $H_c(0) = 2.09$ T increases almost linearly up to $\approx 10\%$ at the field of 3.0 T (A. Paduan-Filho, unpublished).

Depletion is an important matter in BEC because the dissipation effects of non-condensed bosons leads to the creation of solitons and vortices in diluted BECs.

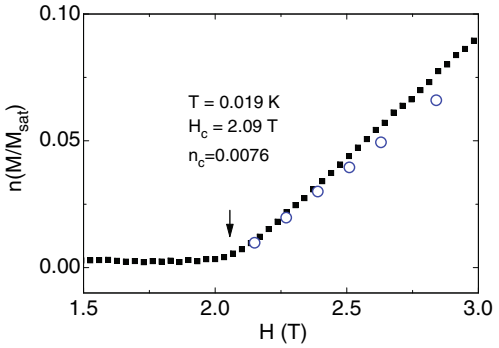

Fig. 11 (*Color online*) Magnetization density at $T = 0.019$K as a funtion of the field. The *filled squares* represent the measured densities. The *open symbols*, representing the condensed bosons, are obtained from (14)

In DTN, an insulating system, this effect has not been observed.

4.16 Theoretical Methods

Almost throughout, the measurements are compared with quantum Monte Carlo data. The simulations agree exceptionally well with the experiments. Some measurements also are correctly fitted by analytic expressions. The values for the DTN parameters refined via QMC and ESR are $D = 8.9$ K, $J_c = 2.2$ K and $J_{ab} = 0.18$ K [37].

With an alternative approach using the diagram technique, one finds an expression for the magnetic phase boundary. Taking into account the coupling constant between the two different tetragonal sublattices, the following set of parameters fit the experimental data very well: $D = 7.72$ K, $J_c = 1.86$ K, $J_{ab} = 0.2$ K, and $V_{\text{intra-sub}} \approx 0.1$ K [45].

4.17 Semi-Hard-Core Boson Model

Both $TlCuCl_3$ and $BaCuSi_2O_6$ have a strong antiferromagnetic coupling between the two $S = 1/2$ spins in each Cu dimer, forming an $S = 0$ singlet ground state separated by a gap J from the $S = 1$ excited triplet. The hard-core model describes the experimental symmetry-induced phase diagram of these systems very well. In DTN this model describes the behavior of the transitions only at low temperatures, $T < 0.2$K, and low fields, $H \lesssim H_{c1}$. An alternative approach can be used to describe the asymmetry of the phase diagram at high fields mapping the $S = 1$ system onto a gas of semi-hard-core bosons. This asymmetry is attributed to the influence of the highest energy level and is not expected for the effective model with $S = 1/2$. In this model the maximum boson population is limited to two per lattice

site. More studies focus on the analysis of the upper critical field and a self-consistent theory [46, 47].

4.18 Two-Magnon Bound States

Theoretical and experimental systematic high-field ESR studies of DTN have been presented with special emphasis on single-ion two-magnon bound states. To clarify some remaining discrepancies between theory and experiment, we analyzed the frequency-field dependence of the magnetic excitations in this material. In particular, a more comprehensive interpretation of the experimental signature of single-ion two-magnon bound states is shown to be fully consistent with theoretical results. Moreover, we have clarified the structure of the ESR spectrum in the so-called intermediate phase. The experimental part was performed at the National High Magnetic Field Laboratory, Tallahassee [48].

5 Summary

We presented an experimental review of the recently observed behavior of DTN associated with BEC phenomena. These experiments provide opportunities for an introductory study of the BEC of magnons in insulating compounds when bosons are induced by an applied magnetic field. The simple magnetic structure of DTN enables experiments in field and temperature regions that are easily accessible in the laboratory. As shown in the theoretical outline presented here, the many-body aspects of BEC are reduced to an effective single-particle description, where interactions give rise to an additional potential proportional to the local particle density. This model allows characterizing the condensation of magnons at low temperatures through parameters such as critical exponents, analysis of the boson density, boson interaction strength, boson mass, depletion, etc. Although this hard-core model describes the low-field behavior of DTN very well, the whole phase diagram can be exactly explained by quantum Monte Carlo simulations with a semi-hard-core model.

The purpose of this review was to describe experiments that go beyond the mean-field theory and explore effects that modify the transition to the field-induced magnetic phase.

Finally, we note that the research in this field has not been limited to condensed matter, but was extended to the applications in nuclear physics, astrophysics, and particle physics.

Acknowledgements The success of the realizing so many experiments on DTN is the result of a collective effort of expertise in the field of magnetism and low temperature. I especially appreciate the stimulating discussions with Vivien Zapf, Marcelo Jaime, Liang Yin, and Tommaso Roscilde throughout the friendly collaboration on the experimental research of BEC. Many other researchers were involved in the studies listed here, including important support by theoretical works.

Investigating the Bose–Einstein condensation in quantum magnets is part of the author's research program, which is supported by FAPESP and CNPq at the Solid-State and Low-Temperature Laboratory of the University of São Paulo. Part of this work was performed at the National High Magnetic Field Laboratory, which is supported by National Science Foundation Cooperative Agreement No. DMR-0654118, the State of Florida, and the U.S. Department of Energy.

References

1. H. Shi, A. Griffin, Phys. Rep. **304**, 1 (1998)
2. T. Giamarchi, C. Ruegg, O. Tchernyshyov, Nat. Phys. **4**, 198 (2008)
3. M.B. Stone, C. Broholm, D.H. Reich, P. Schiffer, O. Tchernyshyov, P. Voderwisch, N. Harrinon, New J. Phys. **9**, 31 (2007)
4. J.O. Andersen, Rev. Mod. Phys. **76**, 599 (2004)
5. G. Baym, J.P. Blaizot, M. Holzmann, F. Laloe, D. Vautherin, Eur. J. Phys. B. **24**, 107 (2001)
6. T. Giamarchi, A.M. Tsvelik, Phys. Rev. B **59**, 11398 (1999)
7. T. Nikuni, M. Oshikawa, A. Oosawa, H. Tanaka, Phys. Rev. Lett. **84**, 5868 (2000)
8. I. Affleck, Phys. Rev. B **43**, 3215 (1991)
9. A.I. Bugrij, V.M. Loktev, J. Low Temp. Phys. **33**, 37 (2007)
10. I. Bloch, J. Dalibard, W. Zwerger, Rev. Mod. Phys. **80**, 885 (2008)
11. M.H. Anserson, J.R. Ensher, M.R. Matthews, C.E. Wieman, E.A. Cornell, Science **269**, 198 (1995)
12. N. Kawashima, J. Phys. Soc. Jpn. **74**(Supp.), 145 (2005)
13. S.E. Sebastian, N. Harrison, C.D. Batista, L. Balicas, M. Jaime, P.A. Sharma, N. Kawashima, I.R. Fisher, Nature **441**, 617 (2006)
14. V.S. Zapf, D. Zocco, B.R. Hansen, M. Jaime, N. Harrison, C.D. Batista, M. Kenzelmann, C. Niedermayer, A. Lacerda, A. Paduan-Filho, Phys. Rev. Lett. **96**, 077204 (2006)
15. E. Orignac, R. Citro, T. Giamarchi, Phys. Rev. B **75**, 140403(R) (2007)
16. J. Kasprzak, M. Richard, S. Kundermann, A. Baas, P. Jeambrun, J.M.J. Keeling, F.M. Marchetti, M.H. Szymanka, R. Andre, J.L. Staehli, V. Savona, P.B. Littlewood, B. Deveaud, L.S. Dang, Nature **443**, 409 (2006)
17. J. Ling, J.P. Wolfe, Phys. Rev. Lett. **71**, 1222 (1993)
18. S.M. Rezende, Phys. Rev. B **79**, 17441 (2009)
19. V.E. Demidov, O. Dzyapko, S.O. Demokritov, G.A. Melkov, A.N. Slavin, Phys. Rev. Lett. **100**, 047205 (2008)
20. F. Yamada, T. Ono, H. Tanaka, G. Misguishi, M. Oshikawa, T. Sakakibara, J. Phys. Soc. Jpn. **77**, 013701 (2008)
21. A. Paduan-Filho, K.A. Al-Hassanieh, P. Sengupta, M. Jaime, Phys. Rev. Lett. **102**, 077204 (2009)
22. A. Paduan-Filho, R.D. Chirico, K.O. Joung, R.L. Carlin, J. Chem. Phys. **74**, 4103 (1981)
23. A. Paduan-Filho, X. Gratens, N.F. Oliveira Jr., J. Appl. Phys. **95**, 7537 (2004)

24. H. Tanaka, F. Yamada, T. Ono, T. Sakakibara, Y. Uwatoko, A. Oosawa, K. Kakurai, K. Goto, J. Magn. Magn. Mater. **310**, 1343 (2007)
25. G. Misguich, M. Oshikawa, J. Phys. Soc. Jpn. **73**, 3429 (2004)
26. H. Enomoto, M. Okumura, Y. Yamanaka, Ann. Phys. **321**, 1892 (2006)
27. J. Sirker, A. Weisse, O.P. Sushikov, J. Phys. Soc. Jpn. **74**(Suppl.), 129 (2005)
28. M. Matsumoto, B. Normand, T.M. Rice, M. Sigrist, Phys. Rev. Lett. **89**, 077203 (2002)
29. J. Sirker, A. Weisse, O.P. Sushkov, Europhys. Lett. **68**, 275 (2004)
30. S.R.A. Salinas, *Introduction to Statistical Physics*, chap. 10 (Springer, New York, 2001)
31. R.K. Pathria, *Statistical Mechanics*, 2nd edn., chap. 7 (Butterworth-Heinemann, Oxford, 2001)
32. A. Paduan-Filho, X. Gratens, N.F. Oliveira Jr., Phys. Rev. B. **69**, 020405(R) (2004)
33. Y. Kohama, A.V. Sologubenko, N.R. Dilley, V.S. Zapf, M. Jaime, J.A. Mydosh, A. Paduan-Filho, K.A. Al-Hassanieh, P. Sengupta, S. Gangadharaiah, A.L. Chernyshev, C.D. Batista, Phys. Rev. Lett. **106**, 037203 (2011)
34. D. Reyes, A. Paduan-Filho, M.A. Continentino, Phys. Rev. B **77**, 052405 (2005)
35. S.A. Zvyagin, J. Wosnitza, A.K. Kolezhuk, V.S. Zapf, M. Jaime, A. Paduan-Filho, V.N. Glazkov, S.S. Sosin, A.I. Smirnov, Phys. Rev. B **77**, 092413 (2008)
36. S. Cox, R.D. McDonald, M. Armanious, P. Sengusta, A. Paduan-Filho, Phys. Rev. Lett. **101**, 087602 (2008)
37. S.A. Zvyagin, J. Wosnitza, C.D. Batista, M. Tsukamoto, N. Kawashima, J. Krzystek, V.S. Zapf, M. Jaime, N.F. Oliveira Jr., A. Paduan-Filho, Phys. Rev. Lett. **98**, 047205 (2007)
38. O. Chiatti, A. Sytcheva, J. Wosnitza, S. Zherlitsyn, A.A. Svyagin, V.S. Zapf, M. Jaime, A. Paduan-Filho, Phys. Rev. B **78**, 094406 (2008)
39. A. Paduan-Filho, K.A. Al-Hassanieh, P. Sengupta, V.S. Zapf, M. Jaime, A. Lacerda, M. Kenzelmann, J. Appl. Phys. **105**, 07D501 (2009)
40. V.S. Zapf, V.F. Correa, P. Sengupta, C.D. Batista, M. Tsukamoto, N. Kawashima, P. Egan, C. Pantea, A. Migliori, J.B. Betts, M. Jaime, A. Paduan-Filho, Phys. Rev. B **77**, 020404 (2008)
41. L. Yin, J.S. Xia, V.S. Zapf, N.S. Sullivan, A. Paduan-Filho, Phys. Rev. Lett. **101**, 187205 (2008)
42. T. Roscilde, S. Haas, Phys. Rev. Lett. **99**, 047205 (2007)
43. Y. Rong et al., arXiv:1109.4403v2 (2011)
44. The boson mass was calculated by M. Kenzelmann from the neutron-scattering data in Ref. [14]. Since at low temperature only the bottom of the magnon band is thermally excited around one minimum, m can be evaluated from the curvature of the band structure around this point. The dispersion is given by $E = \Delta + c^2k^2$, where Δ is the excitation gap c describes the increase in the dispersion as a function of the wave-vector k in lattice units. Writing $E_c = p^2/(2m)$, the obtained mass is $m = (1/2)(2\pi\hbar/(a/c))^2 = 3.7 \times 10^{-25}$g
45. A.V. Sizanov, A.V. Syromyatnikov, Phys. Rev. B **84**, 054445 (2011)
46. H.T. Wang, Y. Wang, Phys. Rev. B **71**, 104429 (2005)
47. K.K. Ng, T.K. Lee, Phys. Rev. B **73**, 014433 (2006)
48. C. Psaroudaki, S.A. Zvyagin, J. Krzystek, A. Paduan-Filho, X. Zotos, N. Papanicolaou, Phys. Rev. B **85**, 104429 (2012)